Frequency conversion in two-dimensional photonic structure

Babic, L.

Chapter 6

Second harmonic generation in transmission from photonic crystals on a gel substrate

6.1 Introduction

Increasing the efficiency of frequency conversion processes has always been an important goal of nonlinear optics. As long as phase-matching conditions are satisfied, a higher nonlinear conversion efficiency can be achieved by either focusing the light or by using a material with a larger nonlinear susceptibility [29]. The phase-matching condition ensures that all the waves generated in the material are in phase, and therefore add up constructively. For most nonlinear media this condition is not automatically satisfied due to material dispersion. Common ways to phase-match the nonlinear interaction are to use temperature tuning or angle tuning of a birefringent nonlinear crystal, e.g., BBO, KTP, or $LiNbO_3$. Unfortunately, this method cannot be applied to optically isotropic materials with a much larger nonlinear susceptibility. This is the case with some III-V semiconductor materials. For example, gallium arsenide (GaAs) has a more than 70 times larger effective second-order nonlinear susceptibility $\chi^{(2)}_{eff}$ than that of BBO but is not birefringent.

Bloembergen et al. [33] were the first to propose a structure with periodically alternating layers of low and high refractive index as a way to satisfy the phase-matching condition. For this structure, an existing phase mismatch can be compensated by adding or subtracting an appropriate reciprocal lattice vector $\mathbf{G}$ of the photonic lattice. This is called quasi-phase-matching. The nonlinear conversion efficiency can be further enhanced significantly by a strong spatial confinement of the optical fields which enhances the field inten-

sities. This has been demonstrated by Scalora et al. [46] for the case of second harmonic generation (SHG) from one-dimensional periodic GaAs/AlAs structures where the enhancement of the second harmonic (SH) signal is achieved by confining both the fundamental and second harmonic optical fields.

Cowan et al. [47] showed theoretically how to use leaky modes of a free-standing two-dimensional photonic crystal slab to achieve both quasi-phase-matching and strong spatial confinement. Leaky modes couple incident light from the surrounding media to a guided mode of the slab via diffraction from the photonic lattice. Using a Green's function formalism, the authors calculated an enhancement of SH signal in reflection of more than 6 orders of magnitude compared to the SH signal off-resonance. An experimental investigation by Mondia et al. [48] resulted in an enhancement of the second harmonic signal generated in reflection from a two-dimensional GaAs photonic crystal slab on an Al_2O_3 cladding layer. The SH signal was generated by focusing a tunable laser with short pulses (150 fs) to a 35 μm spot on the sample. By tuning the laser frequency and the angle of incidence authors investigated the enhancement of the SH signal. When both the fundamental and the second harmonic wave are resonant with the leaky modes of the structure, an enhancement of more than 1200 times compared to the noise floor was measured.

Torres et al. [49] present a theoretical and experimental study of the second harmonic signal generated in reflection from a one-dimensional GaN photonic crystal. They report an enhancement of more than 5000 times compared to an unpatterned GaN slab when both the fundamental and the second harmonic wave are resonant with the leaky modes of the structure. When only the fundamental beam is resonant with the structure, the enhancement is significantly reduced to a factor of 350.

In this chapter we study the influence of leaky modes on the second harmonic generation from a two-dimensional $Al_{0.35}Ga_{0.65}As$ photonic crystal slab on a transparent gel substrate. Compared to earlier experiments in literature [48, 49] a narrow linewidth pulsed laser at 1.535 μm is collimated rather than focused on the sample and the SH signal is measured in transmission instead in reflection. The resonant coupling of both the fundamental and SH wave to the leaky modes of the structure is probed by tuning the angle of incidence. In contrast to the work presented in References [48, 49] where the condition of double resonance was achieved at oblique angles of incidence, our structure is doubly resonant at normal incidence. At normal incidence, the second harmonic signal is enhanced by a factor 10000 relative to the non-resonant signal. The double resonance condition at normal incidence combined with the high enhancement of the SH signal in transmission holds promise for collinear

down-conversion [102, 103].

Compared to earlier experiments [48,49], our experiments clearly show the effect of the resonant coupling of the second harmonic waves to leaky modes of the structure. By increasing the angle of incidence the fundamental beam is tuned away from resonance, resulting in a decrease of the second harmonic signal. However, at angles of incidence of $\pm$ 9.1° two local maxima are clearly observed in the experimental second harmonic signal.

We use a coupled mode theory [60, 100] to explain the main features of the measured second harmonic signal as a function of the angle of incidence. Within this theory, each of the leaky modes of the photonic crystal is treated as a resonance, and the SH signal in transmission depends on how efficiently the fields at the fundamental and the second harmonic frequency couple in or out of these resonances, and on the phase mismatch. Unlike numerical methods such as finite difference time domain calculations or a Green's function approach, our approach offers direct insight into the underlying physical mechanism. More importantly, our simple model uses parameters that are easily obtained by independent measurements of the linear as well as the nonlinear optical properties of the system instead of assuming parameters of an ideal two-dimensional photonic crystal slab. This makes the model immediately applicable to realistic experimental structures that have a finite size and very likely a number of fabrication imperfections. We show that the measured second harmonic signal cannot be explained by considering the resonant coupling at only the fundamental frequency, and that resonant effects at the second harmonic frequency have to be included.

6.2 Sample preparation

Photonic crystal slabs with a square lattice of holes with a hole radius of $\sim$ 150 nm and a lattice constant $a = 820$ nm were fabricated in a commercially grown AlGaAs layer structure [51] using a combination of e-beam lithography and reactive ion etching techniques. The samples were fabricated using the facilities of the Kavli Nanolab Delft. The layers of the AlGaAs layer structure are deposited on a <100> GaAs substrate and consist of a 1 μm thick Al rich $Al_{0.7}Ga_{0.3}As$ layer, a 150 nm thick Ga rich $Al_{0.35}Ga_{0.65}As$ layer, and a 100 nm thick GaAs capping layer. The composition of the slab layer is chosen to render the structure optically transparent at both the fundamental (1535 ± 1 nm) and second harmonic wavelength (767.5 ± 0.5 nm). To create the hole pattern, a 150 nm silicon nitride layer is deposited on top of the structure and serves as a mask during the final reactive ion etching step. The lattice of holes is created

by e-beam lithography in a $\sim$ 500 nm thick layer of positive tone e-beam resist, ZEP 520A [52], and transferred into the nitride mask layer using a low pressure reactive ion etching step in a CHF_3/Ar plasma. After removal of the e-beam resist in a low pressure O_2 plasma, the hole pattern is etched deep into the AlGaAs heterostructure in a $BCl_2/Cl_2/N_2$ reactive ion etch process at 100 W RF power, a pressure of ~ 4.5 μbar, and flow rates of 15, 7.5, and 10 sccm respectively. The nitrogen flow in this process was optimized to create near vertical side walls of the holes. After etching the holes, the nitride mask is removed using the CHF_3/Ar etching procedure described above.

To ensure a nonzero efficiency for second harmonic generation, the ΓX direction of the photonic lattice is deliberately rotated relative to the crystallographic <100> direction of the AlGaAs of the slab layer by an angle of $\sim 22.5°$. Therefore, the incident electric field of the fundamental is never along a crystallographic axis of the AlGaAs and the effective nonlinearity is nonzero. Collinear second harmonic generation along one of the crystallographic directions is forbidden due to the $4\bar{3}$m symmetry of the GaAs lattice [29].

To create a freestanding membrane the residual oxide layer is first removed by dipping the sample in 15:1 deionized H_2O:buffered hydrofluoric acid (BHF) solution for 15 sec. The sample is then placed in a 3:1 citric acid:H_2O_2 solution for 120 sec to selectively remove the GaAs capping layer. The freestanding membrane is created by etching the sacrificial $Al_{0.7}Ga_{0.3}As$ layer in a concentrated 1:4 HF (40%):H_2O solution for 60 sec followed by a rinsing step in pure water and critical point drying. The resulting freestanding membrane covers an area of $\sim 300\times300$ μm^2. Finally, the membrane is transferred to a transparent gel layer [80] with a refractive index of 1.4 on a standard microscope slide, as described in Chapter 4 of this thesis. As a result, an almost perfectly flat membrane which allows for reflection as well as transmission measurements is created.

6.3 Experiment

Figure 6.1 shows the setup used for both second harmonic generation and linear transmission measurements. Alternating between the two experiments is done by flipping both mirrors (flip mirrors) either "down" for second harmonic generation or "up" for linear transmissivity measurements. The second harmonic is generated by a Q-switched Cobolt Tango laser which has a specified center wavelength of 1535 ± 1 nm, and a narrow linewidth < 0.04 nm. The laser produces pulses with a typical duration of ≈ 3.8 ns (full width at half maximum) at a repetition rate of 5 kHz. The generated signal at second har-

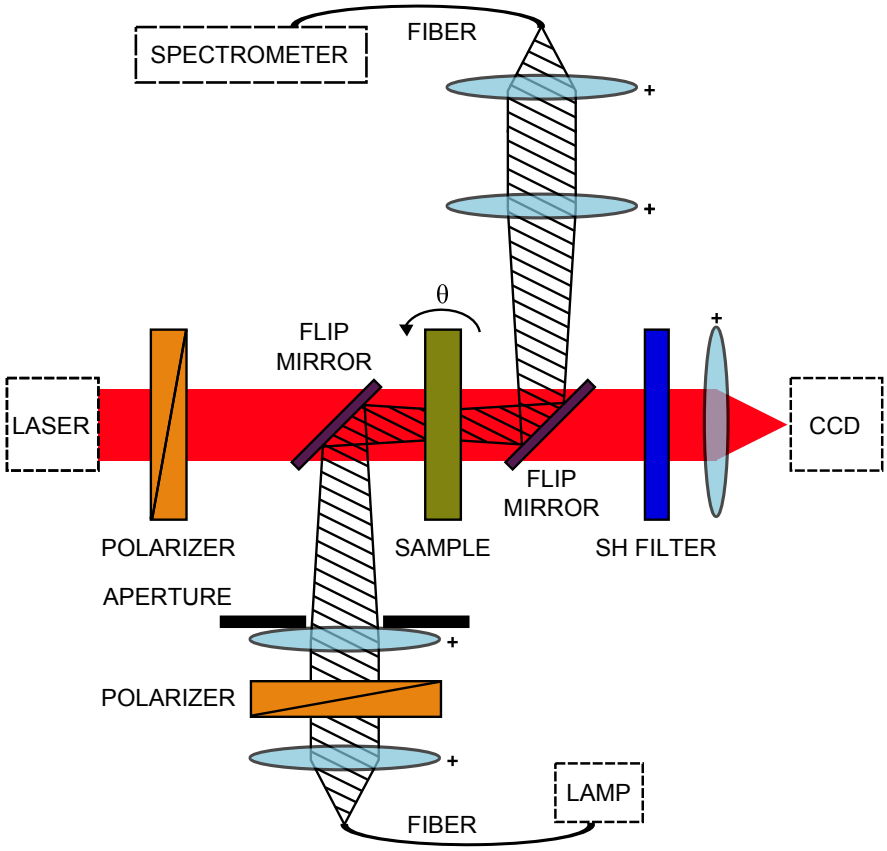

Figure 6.1. Setup used for second harmonic generation and linear transmission measurements. A fiber-coupled lamp and a spectrometer are used for linear transmission measurements, while a pulsed laser operating at 1.535 μm and a CCD camera equipped with a bandpass filter (SH filter) are used for second harmonic measurements. The polarization of the incident beam is set by a Glan-Thompson polarizing beamsplitter cube, and the angle of incidence θ is controlled by placing the sample on a motorized rotation stage. For linear transmission measurements an aperture in the beam limits the angular spread of the incoming light beam. Flip mirrors are used to alternate between the two measurements.

monic wavelength is measured in transmission by an Apogee Alta U1 Peltier cooled CCD camera. Rather then being strongly focused, the fundamental beam is collimated by a lens (not shown), and has a waist of ~ 0.5 mm, and a corresponding half-angular width of ~ 1 mrad. A 25 nm wide bandpass filter (Andover 766FS10-25) centered at a wavelength of 766.5 nm (sh filter) is placed in front of the silicon CCD camera to filter out the fundamental beam. The polarization of the incident fundamental beam is set to either s or p using a Glan-Thompson polarizing beamsplitter cube. Furthermore, a half-wave plate is placed before the polarizer (not shown) to adjust the power at the fundamental wavelength that is incident on the sample. Typically, an average power of ~ 10 mW is used in the experiments.

Linear transmission measurements are performed for wavelengths between 650 and 1700 nm using white light from a halogen lamp coupled to a 50 μm multimode fiber. The output of this fiber is imaged onto the sample with a 2 times magnification to create a 100 μm spot on the sample. The transmitted light is collected into a 400 μm fiber and then sent to a fiber-coupled grating spectrometer. Visible light is detected with a silicon CCD array spectrometer (Ocean Optics USB2000) with a spectral resolution of ≈ 1.5 nm, while the spectrum in the near infrared is detected with an InGaAs array spectrometer (Ocean Optics NIR512) with a ≈ 3 nm spectral resolution. The measurements are done with a very low numerical aperture of the incident beam of NA ≈ 0.01, set by inserting an aperture in the beam path. A Glan-Thompson polarizing beamsplitter cube in a parallel part of the beam is used to measure the transmission of both s- and p-polarized light as a function of wavelength and angle of incidence.

6.4 Results and discussion

The linear transmission and reflection spectra of two-dimensional photonic crystal slabs are well-known, and show a number of asymmetric, dispersive lineshapes [58, 59] due to the coupling of the incident light to one of the leaky modes of the photonic crystal slab via diffraction from the photonic lattice. The coupling of a continuum of modes to a single resonant channel leads to interference between the direct (non-resonant) and indirect (resonant) channel, as was first described by Fano [66]. For a photonic crystal slab, the direct channel corresponds to the Fresnel reflection of the slab, while the resonant channel is created by diffraction of incoming light from the regular photonic lattice into a guided mode of the structure [60].

Figure 6.2 shows a gray scale plot of the measured transmission as a func-

tion of frequency (vertical axis) and the in-plane wave vector $k_{||}$ (horizontal axis), for both s- (a) and p-polarized (b) incident light. The crystal is oriented so that the parallel component of the wave vector $k_{||}$ is along the crystallographic ΓM direction of the photonic lattice. The dark lines that are clearly visible in the figure correspond to the minima of the Fano lineshapes of the leaky modes. The dashed red and the dash-dot blue horizontal lines in the figure indicate the frequencies of the fundamental and the second harmonic.

The experimental transmission spectra $T(\nu) = |t(\nu)|^2$ in the wavelength range between 1400 and 1700 nm (i.e., frequencies ν between 0.48 and 0.58 c/a) are well described by two independent Fano resonances:

$$t(\nu) = t_D(\nu) + \frac{A_1\Gamma_1}{(\nu-\nu_1)+i(\Gamma_1+\gamma_1)} + \frac{A_2\Gamma_2}{(\nu-\nu_2)+i(\Gamma_2+\gamma_2)}, \tag{6.1}$$

where $t_D(\nu)$ is the frequency dependent transmission through the slab given by the Fresnel coefficients of the layered medium. We assume that this direct

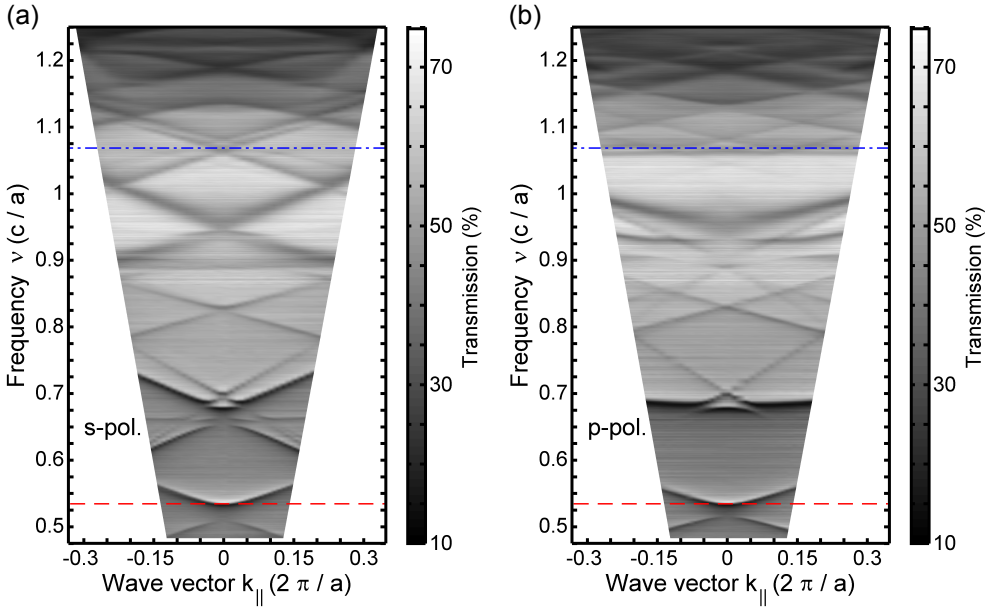

Figure 6.2. Gray scale plot of the measured transmission as a function of frequency (vertical axis) and wave vector $k_{||}$ (horizontal axis). Measurements are shown for s- (a) and p-polarized (b) incident light with $k_{||}$ along the ΓM symmetry direction of the square lattice. The dashed red and the dash-dot blue lines indicate the frequencies of the fundamental and the second harmonic light.

contribution can be approximated well by a linear function over this relatively small frequency range. The parameters $A_{1,2}$ and $\nu_{1,2}$ denote the amplitudes and resonance frequencies of the two modes, while $\Gamma_{1,2}+\gamma_{1,2}$ give the linewidths of the resonances. The radiative coupling to the mode is characterized by $\Gamma_{1,2}$. The loss, quantified by $\gamma_{1,2}$ includes both higher order diffraction as well as scattering loss due to imperfections of the structure. Accordingly, the quality factors of the modes are given by $Q_{1,2} = \nu_{1,2}/(2(\Gamma_{1,2} + \gamma_{1,2}))$ [68]. Figure 6.3 shows the frequencies $\nu_{1,2}$ as a function of the in-plane wave vector $k_{||}$ for both s- (blue circles) and p-polarized light (red diamonds). The frequencies display a clear avoided crossing caused by Bragg type scattering from the periodic array of holes. At normal incidence the leaky modes of the structure are

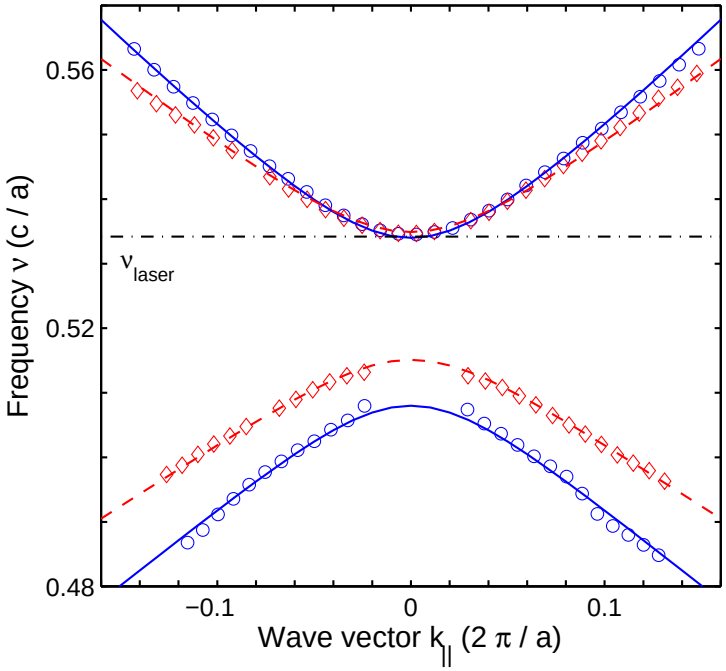

Figure 6.3. Dispersion relations of the lowest four leaky modes for the in-plane wave vector $k_{||}$ oriented along the ΓM direction of the square lattice. Each mode couples to the structure via an addition of one of the four (1,0) reciprocal lattice vectors. The measurements show two modes for both s- (blue circles) and p-polarized light (red diamonds). The solid blue and dashed red lines are fits to the experimental data points using a coupled mode theory, as described in the text. The laser (fundamental) frequency is indicated by the black dash-dot line.

resonant with the pulsed laser operating at 1535 nm (frequency 0.5342 c/a).

The avoided crossing between the leaky modes is well described by the coupled mode theory using a 2×2 Hamiltonian matrix [85, 86, 104]

$$H = \begin{pmatrix} E_1 & V \\ W & E_2 \end{pmatrix},$$

where E_1 and E_2 are energy eigenvalues of the uncoupled modes. For a closed system the energy eigenvalues are real, and the matrix H is Hermitian, and the off-diagonal elements are related by $V = W^*$. The eigenvalues of the coupled system lead to an avoided crossing with energies

$$E_{\pm} = \frac{E_1 + E_2}{2} \pm \sqrt{\frac{E_1 - E_2}{2} + VW}.$$

For an open or dissipative system, such as the leaky modes of the photonic crystal slab considered here, the same Hamiltonian can be used to describe the dynamics of the system. Complex-valued energies $E_{1,2} = h\nu_{1,2} + i(\Gamma_{1,2} + \gamma_{1,2})$ contain both the resonance frequency and the linewidth of the leaky photonic modes. Keeping the restriction $V = W^*$ corresponds to so-called internal coupling since the only difference to the Hermitian coupling is that both modes are individually coupled to the continuum. The fully non-Hermitian case with $V \neq W^*$ corresponds to external coupling, where the modes are coupled via the continuum. An important feature of this external coupling is that it creates a mode with a considerably increased lifetime (subradiant mode), and as a consequence a second mode with a shorter lifetime (superradiant mode). As can be seen from Figure 6.3, modes below the laser frequency (ν_{laser}) become subradiant at normal incidence and disappear from the measured transmission spectra.

For our geometry the leaky modes are excited via diffraction using one of the four $(1, 0)$ reciprocal lattice vectors. For a parallel component of the wave vector in the ΓM $(1, 1)$ direction, the dispersion of the modes of the uncoupled system are obtained by folding the dispersion relation of the fundamental TE waveguide mode. The resulting dispersion relations of the uncoupled modes $\nu_{1,2}$ can be expressed in dimensionless units as:

$$\nu_{1,2} = \nu_0 \sqrt{\left(1 \pm \frac{\alpha k_{||}}{\sqrt{2}}\right)^2 + \left(\frac{\alpha k_{||}}{\sqrt{2}}\right)^2}, \tag{6.2}$$

where ν_0 is the center frequency at normal incidence, and α is a dimensionless parameter that we introduced to control the slope $\partial\nu_{1,2}/\partial k_{||}$. The physical

interpretation of this parameter is that the phase velocity ($\propto \nu/k$) and the group velocity ($\propto \partial\nu/\partial k$) are different.

The avoided resonance crossing in Fig. 6.3 is well described by a center frequency of 0.5210±0.0001 and a frequency splitting of 0.0130±0.0002 for s-polarized light, and a center frequency of 0.5250±0.0001 and a frequency splitting of 0.0099±0.0001 for p-polarized light. The corresponding values for α are 0.733±0.004 and 0.577±0.002 respectively. The resulting dispersion using this relatively simple model is represented by the solid lines for s-polarized light and with dashed lines for p-polarized light in the figure. We stress that the complete band structure of the leaky modes can be obtained by using for instance finite difference time domain (FDTD) simulation software package MEEP [61]. These calculations will correctly predict the dispersion of the modes and the coupling between the s- and p-polarized modes, but do not give physical insight. Our model gives an analytical expression for the resonance frequency of the mode close to the laser (fundamental) frequency. This expression allows to quantify the detuning $\Delta\nu_F(k_{||})$ of the leaky mode relative to the fundamental frequency. It is this detuning, in units of the linewidth of the resonance, that controls the power that leaks into the resonant mode and thus plays an important role in second harmonic experiments. The amplitude of the fundamental field in the leaky mode, excited by the fundamental beam at frequency ν_F, as a function of $k_{||}$ is described by a Lorentzian [60]

$$\begin{aligned} E_F(k_{||}) &\propto \frac{g_1(k_{||})}{(\nu_1(k_{||}) - \nu_F) + i g_1(k_{||})} \\ &= \frac{1}{i + \Delta\nu_F(k_{||})/g_1(k_{||})}, \end{aligned}$$

where $\nu_1(k_{||})$ and $g_1(k_{||})$ represent the dispersion relation and the linewidth of the leaky mode close to the fundamental frequency.

Neglecting resonances at the second harmonic frequency, the intensity of the second harmonic signal I_{SH} as a function of the in-plane wave vector $k_{||}$ is given by

$$I_{SH}(k_{||}) = I_D + \left(\frac{A_F}{1 + \frac{\Delta_F(k_{||})^2}{g_1(k_{||})^2}} \right)^2 . \tag{6.3}$$

The first term in the sum (I_D) represents the direct (non-resonant) contribution, while the second term in the sum represents the resonantly enhanced second harmonic signal with an amplitude A_F.

Figure 6.4 shows the measured second harmonic signal in transmission for various angles of incidence. The data are plotted as a function of the in-plane

wave vector $k_{||}$ of the s-polarized fundamental beam (blue circles). As a result of the resonant coupling to leaky modes of the structure, four distinct peaks are clearly observed in the logarithmic plot at $k_{||} = 0$, $k_{||} = \pm\, 0.085$, and $k_{||} = -0.38 \times 2\pi/a$. At normal incidence ($k_{||} = 0$), the fundamental beam couples resonantly to the structure (see Fig. 6.3), and we measure the highest second harmonic value of 72000 ± 2000 cts/s. This value is more than 10000 × larger than the measured non-resonant contribution of 6.9 ± 0.2 cts/s, determined by taking the averaged value of the measured signal in the interval $k_{||} \in [-0.28, -0.22] \times 2\pi/a$. For $k_{||} \sim 0.25 \times 2\pi/a$ the detuning of the fundamental beam from the leaky modes is maximum. A secondary maximum in the SH signal at $k_{||} = -0.38 \times 2\pi/a$ ($\theta = -45°$) with a value of around 7500 cts/s,

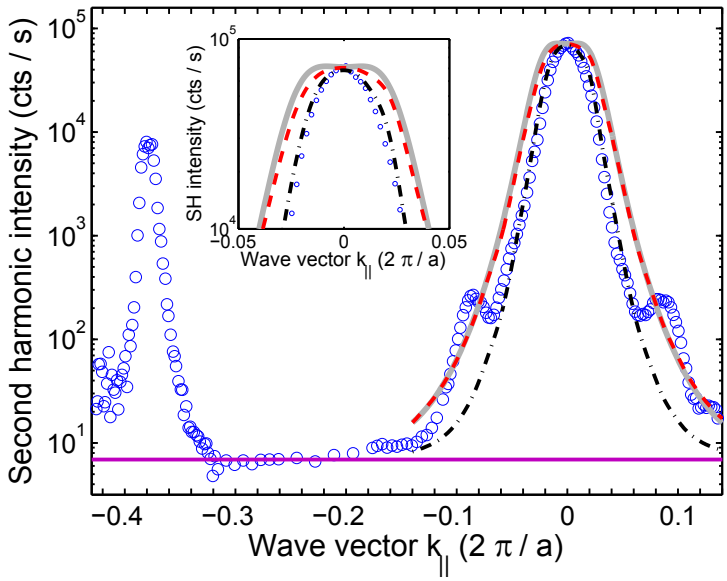

Figure 6.4. Measured second harmonic (SH) intensity in transmission as a function of the wave vector $k_{||}$ of the s-polarized fundamental beam (blue circles). The resonantly enhanced signal is more than 10000 × larger than the non-resonant signal (horizontal line). The solid gray and the dashed red line are calculations taking into account the measured linewidth and dispersion of the mode that is resonant at the fundamental frequency. The dash-dot black line is a fit to the data using the linewidth as the only adjustable parameter. Both models fail to explain the peaks at $k_{||} = \pm\, 0.085 \times 2\pi/a$, which are due to resonant leaky modes at the second harmonic frequency. The inset zooms in on second harmonic intensity at normal incidence ($k_{||} = 0$).

is due to the resonant coupling of the fundamental beam to the (-1,-1) leaky mode of the structure. This resonant contribution to the SH signal disappears for the p-polarized fundamental beam (not shown), because the structure does not support leaky modes at the fundamental frequency in that case (Fig. 4.5 of Chapter 4).

The solid gray line in Figure 6.4 is the second harmonic signal calculated using Equation 6.3 with no adjustable parameters. We use the dispersion relation of the s-polarized leaky mode close to the fundamental frequency as given by Eq. 6.2, and take the measured average quality factor of the leaky mode $Q_1 = 90$ as a measure of the linewidth. For a fundamental frequency $\nu_F = 0.5342$ c/a this translates to a linewidth of $g_1 = \nu_F/(2Q_1) = 0.003$ c/a. For the amplitude of the resonant contribution we substitute $A_F = 268\ \sqrt{\text{cts/s}}$, which is the square root of the measured SH signal at normal incidence, and for the non-resonant contribution we use the measured value of $I_D = 6.9$ cts/s. The calculated function has a local minimum at $k_{||} = 0$ instead of a maximum (see the inset of Fig. 6.4), and therefore doesn't explain the measured SH peak at normal incidence. This artefact occurs because the dispersion relation given by the coupled mode theory crosses the fundamental frequency twice, which is not true for the experimental data. Using a spline fit instead of the coupled mode theory to describe the dispersion relation of the leaky mode results in a second harmonic intensity which has a maximum at normal incidence (dashed red line) and matches better the measured signal. However, the model fails to predict the correct width of the measured SH signal and does not reproduce the peaks at $k_{||} = \pm\ 0.085 \times 2\pi/a$.

The main peak of the SH signal can be explained by Eq. 6.3 if the linewidth of the leaky mode close to the fundamental frequency is used as a fit parameter. The best fit, represented by the black dash-dot line in Figure 6.4, gives a linewidth of $g_1 = 0.00185 \pm 0.00006 \times c/a$, which is a factor 1.6 smaller than the value obtained from the linear transmission measurements.

The two peaks in the SH signal that occur at $k_{||} = \pm\ 0.085 \times 2\pi/a$, and have a value of ≈ 240 cts/s, cannot be explained by a relatively simple model that only considers the leaky mode at the fundamental frequency. As the in-plane wave vector of the incident fundamental beam is tuned away from $k_{||} = 0$ the power of the fundamental in the slab drops, and as a consequence the second harmonic intensity is expected to drop monotonically as well. Instead, the generated second harmonic field in the photonic crystal slab also couples to leaky modes of the structure. This double resonant coupling is the origin of the reduced width of the measured second harmonic signal at normal incidence and of the two additional peaks at $k_{||} = \pm\ 0.085 \times 2\pi/a$.

The incident laser beam couples to the fundamental TE mode of the photonic crystal slab waveguide. This mode has its **E**-field components predominantly in the plane of periodicity [82], i.e., in the x- and y-directions. The nonlinear tensor properties of the material are related to the cubic $4\bar{3}$m symmetry of the AlGaAs crystal. For this crystal symmetry the only nonzero tensor elements are $d_{14} = d_{25} = d_{36}$ [29]. Therefore, the generated second harmonic wave has the main **E**-field component in the z-direction, perpendicular to the plane of periodicity [29], and couples most efficiently to TM waveguide modes. The second harmonic intensity can be written in this case as:

$$I_{SH}(k_{||}) = I_D + \left(\frac{A_F}{1 + \frac{\Delta_F(k_{||})^2}{g_1(k_{||})^2}} \right)^2 \times \frac{1}{1 + \frac{\Delta_{SH}(k_{||})^2}{g_3(k_{||})^2}} \times L^2 \frac{\sin^2(\Delta k L/2)}{(\Delta k L/2)^2}.$$

Here, the first term is the direct contribution from the slab, while the second term is a product of the resonant contribution at the fundamental frequency, the resonant contribution at the second harmonic frequency, and a term related to the phase mismatch Δk between the waveguide modes involved. The phase mismatch $\Delta k = |2\mathbf{k}_{||}(\nu_F) - \mathbf{k}_{||}(\nu_{SH}) + \mathbf{G}|$, where $\mathbf{k}_{||}(\nu_F)$ is the in-plane wave vector of the fundamental beam, and $\mathbf{k}_{||}(\nu_{SH})$ is the in-plane wave vector of the wave at the second harmonic frequency ν_{SH}. The length L is the length of the sides of our square structure. The dispersion relation and the linewidth of the leaky mode close to the second harmonic frequency, $\nu_3(k_{||})$ and $g_3(k_{||})$, define the frequency detuning $(\nu_3(k_{||}) - \nu_{SH})/g_3(k_{||}) = \Delta_{SH}/g_3$, which determines how efficiently the generated second harmonic couples to external radiation. To understand the measured second harmonic signal, it is important to identify the leaky mode to which the second harmonic wave couples.

To find out which TM leaky modes can be excited at the second harmonic frequency, we use the nearly free photon picture introduced by Sakoda et al. [82]. In this picture, the photonic crystal slab is approximated with a dielectric slab with an effective dielectric permittivity that takes into account the effect of holes and different polarizations. The dispersion of the leaky modes of the photonic crystal slab is obtained by folding the dispersion of the waveguide modes of the dielectric slab back to the first Brillouin zone by adding an appropriate reciprocal lattice vector. Figure 6.5 shows the dispersion relation of relevant fundamental TE and fundamental TM leaky modes plotted over the measured transmission spectra for s-polarized light (from Fig. 6.2(a)). Figure 6.6 shows the dispersion relation of relevant fundamental

TE and fundamental TM leaky modes plotted over the measured transmission spectra for p-polarized light (from Fig. 6.2(b)). The dispersion of the TE leaky modes (dash-dot lines) is obtained by folding the dispersion of the fundamental TE waveguide mode of the slab with an effective dielectric permittivity $\epsilon_{TE} = 0.89 \times \epsilon$, where ϵ is the dielectric permittivity of $Al_{0.35}Ga_{0.65}As$ [62]. Similarly, by folding the dispersion of the fundamental TM waveguide mode of a slab with an effective dielectric permittivity $\epsilon_{TM} = 0.95 \times \epsilon$ the dispersion of TM leaky modes (dashed lines) is obtained. Each leaky mode is denoted with a reciprocal lattice vector (G_x, G_y) used for folding of the guided modes back into the first Brillouin zone. For clarity, only the relevant leaky modes at the fundamental and at the second harmonic frequency are shown. The nearly free photon approximation doesn't take into account the interaction between the leaky modes, and as a consequence it cannot describe the frequency splitting between the modes of the photonic crystal slab. As can be seen, good agreement between the nearly free photon picture and measured spectra is obtained away from the crossings.

The horizontal purple lines in Figures 6.5 and 6.6 indicate the fundamental and second harmonic frequencies. The s-polarized fundamental wave couples to a mode of the family of (1,0) TE modes. The figures show that the generated SH signal could couple to one or more modes of the family of (2,1) TM modes at normal incidence. We stress that the leaky modes due to TM waveguide modes are generally less visible in transmission spectra than resonances due to TE modes. Therefore, we need to resort to the nearly free photon picture in order to resolve these modes. In the nearly free photon picture, the family of (2,1) TM modes is 8-fold degenerate at normal incidence, and it is impossible to say with certainty to which modes the second harmonic radiation is most likely to couple to. For nonzero angles of incidence, the dispersions of the (-2,-1) and (1,-2) modes are resonant with the second harmonic frequency. Therefore, we speculate that the generated second harmonic wave couples to one of these modes at angles of incidence of $\theta = \pm\ 9.1°$, indicated by the dotted lines in Figures 6.5 and 6.6. Since the measured second harmonic signal is elliptically polarized, we conclude that the second harmonic wave couples to both s- and p-polarized leaky modes of the structure.

Unfortunately, it is not possible to resolve the dispersion relations and the linewidths for the modes at the second harmonic frequency from the measured transmission spectra. The main reason for this is that there are other resonances due to TE modes around the second harmonic frequency. All these modes interact, and as a consequence the transmission spectra do not consist of isolated and easily recognizable Fano lineshapes superimposed on top of the

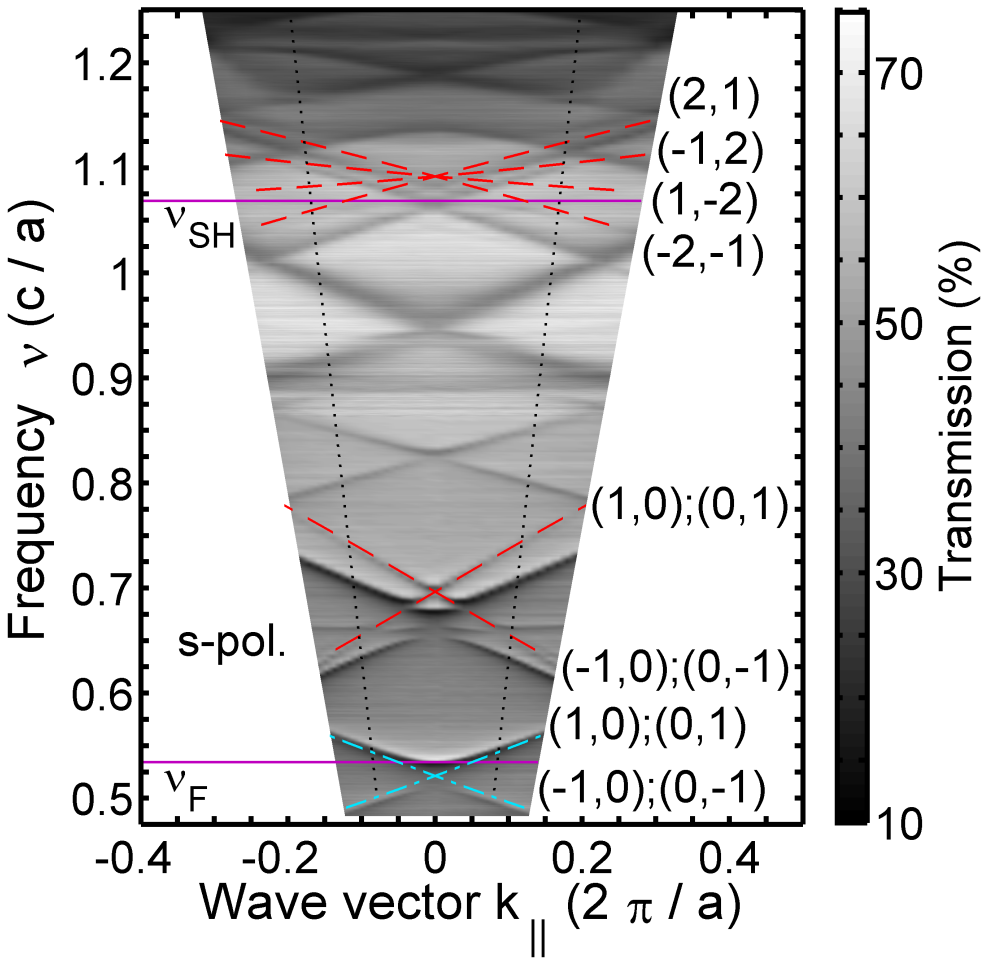

Figure 6.5. Dispersion relation of leaky TE (dash-dot lines) and TM (dashed lines) modes in the nearly free photon picture, plotted on top of the measured transmission data for *s*-polarized light (from Fig. 6.2(a)). The dispersion relations are obtained by folding the dispersions of the fundamental TE and TM waveguide modes of a dielectric slab on a gel back to the first Brillouin zone. The fundamental and second harmonic frequencies, $\nu_F = 0.5342\ c/a$ and $\nu_{SH} = 1.0684\ c/a$, are indicated by horizontal purple lines. The dotted lines indicate constant angles of incidence $\theta = \pm\ 9.1°$.

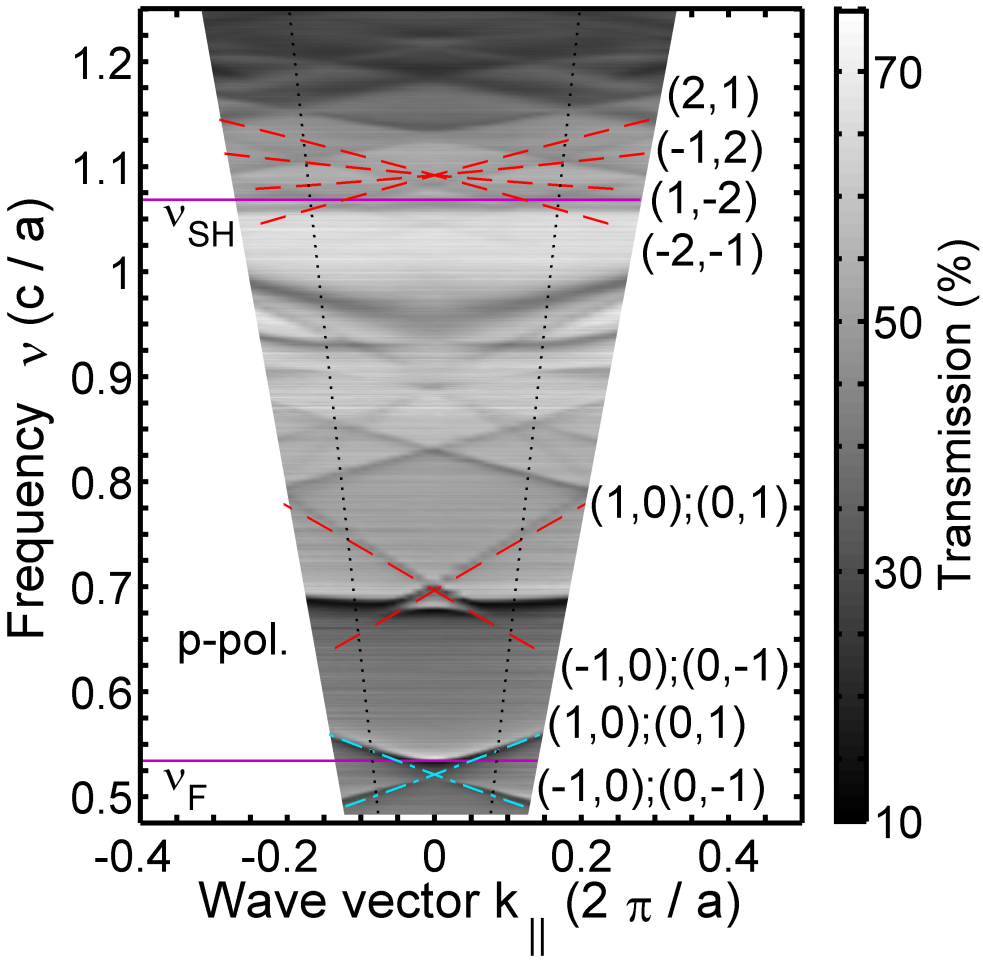

Figure 6.6. Dispersion relation of leaky TE (dash-dot lines) and TM (dashed lines) modes in the nearly free photon picture, plotted on top of the measured transmission data for p-polarized light (from Fig. 6.2(b)). The dispersion relations are obtained by folding the dispersions of the fundamental TE and TM waveguide modes of a dielectric slab on a gel back to the first Brillouin zone. The fundamental and second harmonic frequencies, $\nu_F = 0.5342\ c/a$ and $\nu_{SH} = 1.0684\ c/a$, are indicated by horizontal purple lines. The dotted lines indicate constant angles of incidence $\theta = \pm\ 9.1°$.

Fabry-Perot background.

In principle, the generated second harmonic field can couple to TE leaky modes as well. Unlike TE modes of an ideal, infinitely long photonic crystal, TE leaky modes of the photonic crystal slab can have a small component of the **E**-field perpendicular to the plane of the slab [63], related to the absence of the continuous translational symmetry in the direction perpendicular to the plane of periodicity. This small component of the fundamental electric field perpendicular to the plane of periodicity can give rise to a second harmonic field with an electric field component in the plane of periodicity which can efficiently couple to TE leaky modes. We estimate that this effect is much smaller compared to the contribution to the SH signal due to resonant coupling of the second harmonic waves to TM leaky modes.

6.5 Conclusions

We investigate the influence of leaky modes on the second harmonic signal generated in transmission from a two-dimensional $Al_{0.35}Ga_{0.65}As$ photonic crystal slab on a gel substrate. By tuning the angle of incidence of the fundamental beam we probe the resonant coupling of the fundamental and the second harmonic wave to leaky modes of the structure. At normal incidence, both the fundamental and the second harmonic wave resonantly couple to the structure, and we measure a second harmonic enhancement of more than 10000 $\times$ compared to the measured non-resonant contribution. This is more than eight times larger than the experimental enhancement measured in reflection by Mondia et al. [48]. Two additional maxima can be clearly seen in the measured second harmonic for angles of incidence of $\pm$ 9.1°. We explain this effect by a resonant coupling of the second harmonic wave to leaky modes of the photonic crystal slab. Compared to experimental results reported in References [48, 49], our measurements convincingly show the influence of resonant effects at second harmonic frequency.

Using a relatively simple coupled mode theory rather than full numerical calculations we analyze the effects of resonant coupling of waves at the fundamental and the second harmonic frequency to leaky modes of the structure on the second harmonic generation. This coupled mode approach offers valuable physical insight and is applicable to less-than-perfect structures. This makes it a very useful tool for future analysis and design of both linear and nonlinear optical properties of photonic crystal slabs.